IEEE Photonics Journal
An IEEE Photonics Society Publication

Open Access

Efficient Second Harmonic Generation by Mode Phase Matching in a Silicon Waveguide

Volume 9, Number 3, June 2017

Jiangchuan Huang
Hailong Han
Ang Liu
Hongfei Wang
Xiaoping Liu
Yi Zou
Minghui Lu
Yanfeng Chen

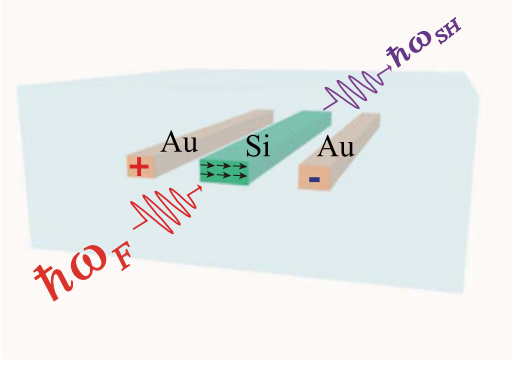

DOI: 10.1109/JPHOT.2017.2697073
1943-0655 © 2017 IEEE

Efficient Second Harmonic Generation by Mode Phase Matching in a Silicon Waveguide

Jiangchuan Huang,[1] Hailong Han,[1] Ang Liu,[1] Hongfei Wang,[1] Xiaoping Liu,[1,2] Yi Zou,[1,2] Minghui Lu,[1,2] and Yanfeng Chen[1,2]

[1]National Laboratory of Solid State Microstructures and College of Engineering and Applied Sciences, Nanjing University, Nanjing 210093, China
[2]Collaborative Innovation Center of Advanced Microstructures, Nanjing University, Nanjing 210093, China

DOI:10.1109/JPHOT.2017.2697073

Manuscript received March 31, 2017; revised April 17, 2017; accepted April 18, 2017. Date of publication April 25, 2017; date of current version May 8, 2017. This work was supported in part by the National Nature Science Foundation of China under Grant 61378009, in part by the National Basic Research Program of China under Grant 2015CB659400, and in part by the Natural Science Foundation of Jiangsu Province under Grant BK20150057 and Grant BK20160631. Corresponding authors: Xiaoping Liu and Yi Zou (e-mail: xpliu@nju.edu.cn; yzou@nju.edu.cn).

Abstract: Bulk silicon possesses no second-order susceptibility ($\chi^{(2)}$), inhibiting second-order nonlinear processes in the emerging silicon photonic platform. Here, we propose a method to overcome this limitation by enabling a third-order ($\chi^{(3)}$) nonlinear mixing scheme between optical waves and an externally applied static electric field inside a silicon waveguide. We show in theory that facilitated by a modal phase-matching scheme efficient second-harmonic generation can be realized under an applied voltage of 65 V, giving rise to an equivalent $\chi^{(2)} = 4.7$ pm/V. We also show that unlike the classical second-harmonic generation, the wavelengths of phase-matched pump and second-harmonic waves are pump-power dependent due to the $\chi^{(3)}$ nature of this process.

Index Terms: Silicon waveguide, second harmonic generation, mid-infrared

1. Introduction

As the complementary metal–oxide semiconductor (CMOS) photonic platform getting mature, the concept of nonlinear lab on a silicon chip is attracting more and more research interests. The ultra-small mode size (on the order of μm^2) of a silicon photonic nanowire, making feasible a high optical pump intensity at low input powers [1], [2]. Coupled with its large third order nonlinear susceptibility, the silicon photonic nanowire has enabled researchers to investigate various nonlinear effects using ultrafast lasers [3], [4]. However, owing to silicon's inversion symmetry, the second-order nonlinear susceptibility cannot be exploited in bulk silicon. Therefore, second-order nonlinear effects, e.g., second-harmonic generation (SHG), spontaneous parametric down conversion, etc., are hardly studied and reported in conventional silicon photonic devices.

Considerable efforts have been devoted to realize second-order nonlinearity in silicon photonic devices. For instance, the surface of bulk silicon, where the silicon's inversion symmetry is naturally broken, can be used to generate second-order nonlinear response [5], [6]. However, the effective second-order nonlinearity in this case is confined to a few atomic layers near surface, and thus, it is

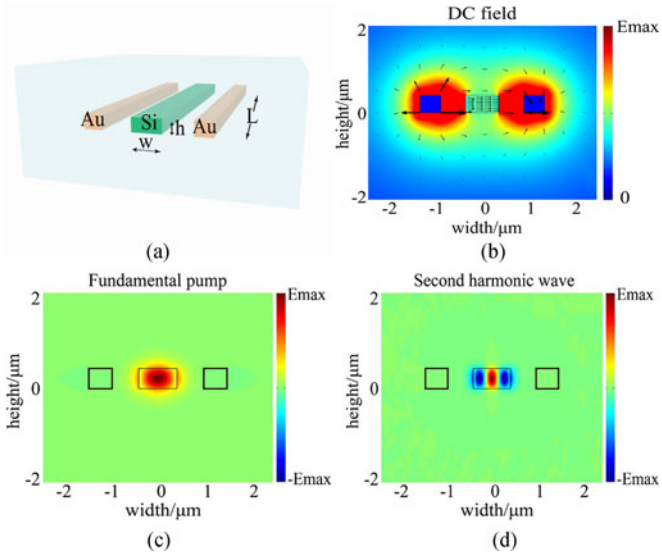

Fig. 1. (a) Schematic of our waveguide configuration. (b) Static electric field with arrows indicating the direction of the field. (c) and (d) Typical mode for fundamental pump and second harmonic waves.

often very weak. Straining bulk silicon to break its inversion symmetry is another feasible approach to induce second-order nonlinear response [7]–[9]. In this case, an effective control and/or tuning of second-order nonlinearity in experiment is often difficult.

2. Waveguide Design

In this paper, we propose a new approach to generate effective second-order nonlinearity in a silicon waveguide by applying an external static electric field across it. Our proposed configuration consists of a silicon channel waveguide and two nearby parallel gold electrodes, which are all buried in silicon dioxide as shown in Fig. 1(a). The silicon waveguide has a fixed height of 400 nm and two electrodes (500 nm $\times$ 400 nm) are separated by 2.5 μm to reduce their interaction with the optical modes in the silicon waveguide. Silicon's intrinsic third-order nonlinearity $\chi^{(3)}$ in this configuration facilitates four-wave mixing according to $P \sim \hat{\chi}^{(3)}\vdots e_l e_m e_n$, where e_l, e_m and e_n represent electric fields of three input interacting optical waves, and P represents the generated nonlinear polarization of the fourth wave. SHG in the silicon waveguide can occur when one of the input optical fields is a static electric field [10]–[12].

Typical static electrical field induced under an applied DC voltage is illustrated in Fig. 1(b). Clearly, the field inside the silicon waveguide has a dominant component parallel to the silicon dioxide substrate. Hence, quasi-TE modes are preferred for a better overlap with the static field and thus better utilization of the silicon's third-order nonlinearity [13] to generate SHG. A modal phase matching scheme between the waveguide's quasi-TE_{00} mode (fundamental pump) and quasi-TE_{20} mode (second-harmonic wave) is used in this study. A typical example of the fundamental pump wave and the corresponding second-harmonic wave is shown in Fig. 1(c) and (d), respectively.

The width of the silicon waveguide is swept from 800 nm to 900 nm to find out an appropriate modal phase-matching condition. Our wavelength of interest for the fundamental pump is between 2300 nm and 2500 nm, where the lower limit helps to avoid silicon's two-photon absorption while the upper limit to avoid excess absorption in the silicon dioxide. The calculated dispersion diagram for the pump and the second-harmonic wave for three typical waveguides are plotted in Fig. 2. Specifically, the width of 830 nm can support the phase matched pump and second-harmonic waves at wavelengths of 2389.5 nm and 1194.75 nm respectively. It is used as a representative example to investigate SHG process.

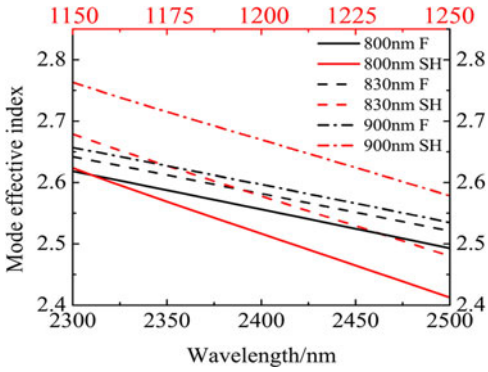

Fig. 2. Effective indices of the fundamental and the second-harmonic waves when the waveguide width is 800 nm, 830 nm, and 900 nm. Here, F and SH represent fundamental pump and the second-harmonic waves, respectively.

3. Theoretical Model and Simulation Results

To characterize the SHG process in our proposed scenario, the theoretical model outlined in [14]–[16] is adapted resulting in the following coupled nonlinear Schrödinger equations (NLSE) for the fundamental wave and second-harmonic wave.

$$\frac{i\partial u_F}{\partial z}+\sum_{n\geq 1}\frac{i^n\beta_n^F}{n!}\frac{\partial^n u_F}{\partial t^n}=-\frac{ic\kappa_F}{2n_{si}v_g^F}(\alpha_{\ln}^F+\alpha_{FC}^F)u_F-\frac{\omega_F\kappa_F}{n_{si}v_g^F}\delta n_{FC}^F u_F-\frac{3\omega_F P_F\Gamma_F}{4\varepsilon_0 A_0 v_g^{F\,2}}|u_F|^2u_F$$
$$-\frac{6\omega_F}{4\varepsilon_0 A_0 v_g^D}\frac{\Gamma_{SH;F,F,D}P_F}{v_g^F}u_{SH}u_D u_F^*\exp(-i\Delta k_l z) \quad (1a)$$

$$\frac{i\partial u_{SH}}{\partial z}+\sum_{n\geq 1}\frac{i^n\beta_n^{SH}}{n!}\frac{\partial^n u_{SH}}{\partial t^n}=-\frac{ic\kappa_{SH}}{2n_{si}v_g^{SH}}(\alpha_{\ln}^{SH}+\alpha_{FC}^{SH})u_{SH}-\frac{\omega_{SH}\kappa_{SH}}{n_{si}v_g^{SH}}\delta n_{FC}^{SH}u_{SH}$$
$$-\frac{3\omega_{SH}}{4\varepsilon_0 A_0 v_g^{SH}}\left(2\frac{\Gamma_{F,SH}P_F}{v_g^F}\right)|u_F|^2u_{SH}-\frac{3\omega_{SH}}{4\varepsilon_0 A_0 v_g^D}\frac{\Gamma_{SH;F,F,D}P_F}{v_g^F}u_F{}^2u_D^*\exp(i\Delta k_l z). \quad (1b)$$

Here, the subscript j = F, SH, D corresponds to the fundamental pump wave, second-harmonic wave and static electric field, respectively, u_j is the normalized pulse envelop, β_n^j is the nth order dispersion term, n_{si}^j is the refractive index of bulk silicon, v_g^j is the group velocity, P_F is the peak power of the fundamental wave, A_0 is the area of the waveguide cross section, and $\alpha_{\ln}^j$ is the linear loss inside the silicon waveguide, and $\Delta k_1 = 2\beta_F - \beta_{SH}$ describes the linear phase mismatch. α_{FC}^j and δn_{FC}^j are free carrier absorption (FCA) and dispersion [17]. κ is the power confinement:

$$\kappa_j=\frac{n_{si}^2\int_{A_0}|e_j|^2dA}{\int n^2(r)|e_j|^2dA} \quad (2)$$

where $n(r)$ is the index in transverse plane, and $e_j \equiv e_j(\omega, r)$ is the electric field distribution of the waveguide mode. In addition, Γ is the waveguide effective third-order nonlinearity defined as

$$\Gamma_j=\Gamma_{jjjj} \quad (3a)$$
$$\Gamma_{jl}=\Gamma_{jllj} \quad (3b)$$
$$\Gamma_{jlmn}=\frac{A_0\int_{A_0}e_j^*\cdot\hat{\chi}^{(3)}(-\omega_j;\omega_l,-\omega_m,\omega_n)\vdots e_l e_m^* e_n dA}{\varsigma_j\varsigma_l\varsigma_m\varsigma_n} \quad (3c)$$

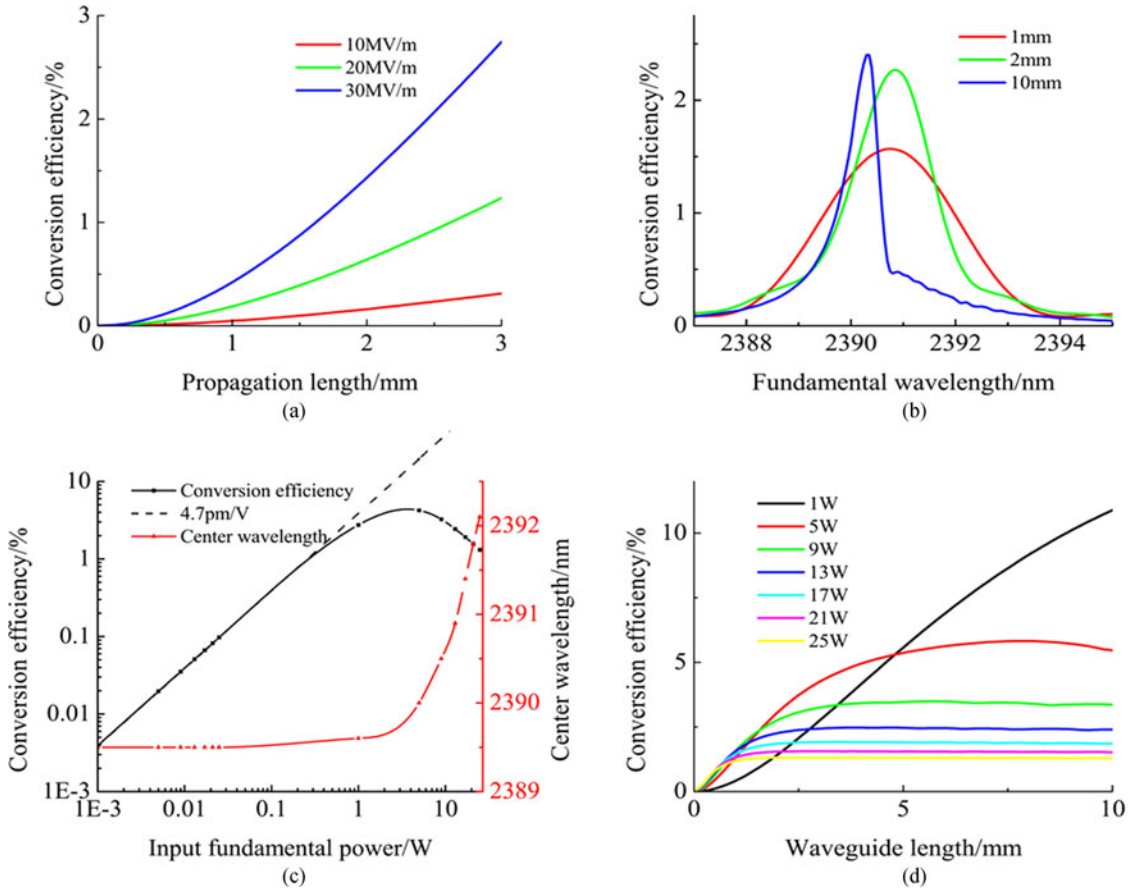

Fig. 3. (a) SHG efficiency vs. propagation length at different static electric field intensities (10 MV/m, 20 MV/m and 30 MV/m). The input pump power is 1 W. (b) SHG efficiency vs. wavelength with different waveguide lengths (1 mm, 2 mm, and 10 mm). The input power for the fundamental pump is 13 W. (c) Peak SHG efficiency and its center wavelength as a function of the pump power for a waveguide length of 3 mm. The dashed line corresponds to the classic $\chi^{(2)}$ SHG model with an equivalent scalar $\tilde{\chi}^{(2)} = 4.7$ pm/V. (d) SHG efficiency vs. waveguide length at different pump power levels.

where $\varsigma_j = (\int n^2(r)|e_j|^2 dA)^{1/2}$, and $\hat{\chi}^{(3)}(-\omega_j; \omega_l, -\omega_m, \omega_n)$ is the silicon's non-degenerated third order susceptibility. $\hat{\chi}^{(3)}(-\omega_j; \omega_j, -\omega_j, \omega_j)$ is approximated by $\hat{\chi}^{(3)}(-\bar{\omega}; \bar{\omega}, -\bar{\omega}, \bar{\omega})$, where $\bar{\omega} = (\omega_j + \omega_l + \omega_m + \omega_n)/4$ is the average angular frequency, for only the degenerated $\hat{\chi}^{(3)}(-\omega_j; \omega_j, -\omega_j, \omega_j)$ for silicon is readily available in literature [10].

Free carrier density is governed by cross two photon absorption (X-TPA) between the fundamental pump and second-harmonic waves and degenerate TPA of the second harmonic wave. Since in our case the SHG efficiency is limited by the linear loss to a few percent as discussion later, the dynamics of free carrier density is dominated by X-TPA and can be expressed as

$$\frac{\partial N}{\partial t} = -\frac{N}{\tau_c} + \frac{1}{\varepsilon_0 \hbar A_0{}^2}\left(\frac{\Gamma''_{F,\,SH} P_F{}^2}{2 v_g^F v_g^{SH}} |u_F|^2 |u_{SH}|^2\right). \tag{4}$$

A hyperbolic-secant pulse is used as the fundamental pump wave and its temporal width is set to be 1 ns to reduce the walk-off between the pump wave and second-harmonic waves. The above coupled NLSEs [see (1a) and (1b)] and carrier rate equation (4) are solved using Runge-Kutta method [18]. As shown in Fig. 3(a), which plots the SHG peak efficiency (defined as the ratio between the peak power of the generated second-harmonic wave and the input fundamental pump wave) as a function of propagation distance at three different static electric field levels, the SHG

process will be more efficient under a stronger static electric field level. Therefore, the peak static electric field used in the silicon waveguide in our following discussion is set below the breakdown field of silicon [19] to a value about 30 MV/m (corresponding to an applied voltage of 65 V), and the propagation loss of all the optical waves is set to an experimentally feasible value, 1 dB/cm [20].

The input fundamental pump intensity is varied to study its impact on the SHG efficiency. Several representative scenarios are investigated and discussed as follows. In the first scenario as shown in Fig. 3(b), where the pump peak power is fixed at 13 W, the peak SHG efficiency is found to be reasonably large with a value about a few percent for all three different waveguide lengths. All pump wavelengths at the peak of the SHG efficiency are found to acquire a red shift from the calculated phase-matched wavelength shown in Fig. 2. This effect is attributed to the negative nonlinear phase shift existing between the fundamental wave and the second-harmonic wave via Kerr effect (self-phase modulation and cross-phase modulation), which can be compensated by having a slightly red-shifted pump wavelength. Notice that increasing the waveguide length by 5 times, i.e. from 2 mm to 10 mm, reduces the amount of red shift of the peak wavelength but barely changes the peak SHG efficiency. This is mainly due to a gradually decreasing pump intensity with the increasing length of propagation in the presence of linear and nonlinear propagation losses. It impacts the underlying SHG in two ways: 1) causing less nonlinear phase shift, which directly translates into a reduced red shift, and 2) reduced SHG efficiency. Furthermore, the wavelength bandwidth for SHG is reduced as the waveguide length increases. This is a common effect routinely observed in nonlinear processes where a phase-matching condition is required.

Next, the pump-power dependent SHG process is investigated and the peak SHG efficiency for a 3 mm silicon waveguide is recorded and plotted in Fig. 3(c). It indicates that for low pump powers (e.g., $<$1 W), where there is negligible nonlinear loss coming from X-TPA and FCA, the SHG efficiency scales nearly linearly with the pump power and the wavelengths of the peak SHG efficiency match well with that predicted by the phase matching curve shown in Fig. 2. This finding is consistent with a classic picture for a $\chi^{(2)}$ SHG model involving material second-order nonlinearity [21]. For high pump powers, the result shows a very different picture. The SHG efficiency in this case increases sub-linearly with the pump intensity before it reaches a maximum about 4.2% and then starts to drop. This behavior is a direct outcome of the competition between the generation and annihilation rate of the second-harmonic photons, both of which are highly dependent upon the pump power along the waveguide. Notice that SHG conversion efficiency as high as tens of percent can be achieved in traditional $\chi^{(2)}$ materials such as $LiNbO_3$ [22]. These materials, however, face serious compatibility issues with modern planar microfabrication processes and integration issues with other chip-based optical components. For photonic integrated platforms [8], [23]–[25], we have found efficiency around a few percent in a non-resonant structure is on the high side. The pump-power dependent SHG efficiency spectra reveal another unique feature of this static electric field assisted SHG process. As shown in the figure, the peak SHG wavelengths stay the same at the low pump powers, but starts to acquire a noticeable red shift at high pump powers, which is unique to this silicon waveguide configuration employing $\chi^{(3)}$ nonlinearity and is not commonly found in the classic $\chi^{(2)}$ SHG model [21], [26], [27]. Nevertheless, fitting the linear region of the pump-power dependent SHG efficiency using the classical $\chi^{(2)}$ SHG model [26] yields an equivalent scalar $\chi^{(2)} = 4.7\,\text{pm/ V}$ in our case. Although this value is small compared with that of commonly used $\chi^{(2)}$ materials, e.g., $LiNbO_3$ [28], our study here clearly illustrates that a high SHG efficiency can be readily attained thanks to an enhanced pump intensity resulted from silicon waveguide's ultra-small modal size. Nevertheless, the turn-around behavior of the SHG efficiency with pump power here suggests that using a high pump power is not the best option for achieving high efficiency. In fact, as seen in Fig. 3(d) that plots the SHG efficiency as a function of waveguide length for a range of pump power levels, the length-dependent efficiency can be strongly influenced by the pump power. At high pump power levels, e.g., here, $\geq$5 W, the SHG efficiency shows a nonlinear optical limiting behavior, forming a plateau region where the efficiency is clamped regardless of the waveguide length. Further examination of the results show that the efficiency at the plateau decreases with the increasing pump power and the plateau forms at a shorter waveguide length with a stronger pump power. For a low pump power, e.g., 1 W, the SHG efficiency increases nearly linearly with

the waveguide length, reaching more than 10% at the length of 10 mm. Therefore, as discussed above, due to the existence of nonlinear loss, high efficiency SHG process could be achieved with relatively low pump power levels at the expense of a prolong waveguide.

4. Conclusion

To conclude, we have outlined a configuration with a strong static electric field across a silicon waveguide to realize efficient SHG. We show that the wavelengths for the phase-matched fundamental wave and the second-harmonic wave can possess a red shift as a result of Kerr effect by a strong pump, which is a unique to such scheme. The externally applied electric field employed in our approach to interact with the optical fields propagating inside the silicon waveguide may enable great flexibility in controlling SHG, which are utterly important in future, for our study opens a door to promising applications in the mid-infrared region, such as electro-optic modulation and simultaneously conversion of mid-infrared signal for low-noise detection in the near-infrared region. By incorporating a chirped grating based phase-matching scheme, the operation band of this SHG process can be further expanded [29], [30], which may find great potentials in mid-infrared spectroscopy, optical communication, photonic quantum systems and integrated optoelectronic circuit [3], [31]–[33].

References

[1] L. Pavesi, *Silicon Photonics*, vol. Topics in Applied Physics. New York, NY, USA: Springer, 2004.
[2] D. J. Lockwood, *Silicon Photonics II*, vol. Topics in Applied Physics. New York, NY, USA: Springer, 2011.
[3] Q. Lin, O. J. Painter, and G. P. Agrawal, "Nonlinear optical phenomena in silicon waveguides: Modeling and applications," *Opt. Exp.*, vol. 15, pp. 16604–16644, Dec. 10, 2007.
[4] J. Leuthold, C. Koos, and W. Freude, "Nonlinear silicon photonics," *Nature Photon.*, vol. 4, pp. 535–544, Aug. 2010.
[5] S. V. Govorkov, V. I. Emelyanov, N. I. Koroteev, G. I. Petrov, I. L. Shumay, and V. V. Yakovlev, "Inhomogeneous deformation of silicon surface-layers probed by 2nd-harmonic generation in reflection," *J. Opt. Soc. Amer. B-Opt. Phys.*, vol. 6, pp. 1117–1124, Jun. 1989.
[6] M. Galli *et al.*, "Low-power continuous-wave generation of visible harmonics in silicon photonic crystal nanocavities," *Opt. Exp.*, vol. 18, pp. 26613–26624, Dec. 6, 2010.
[7] R. S. Jacobsen *et al.*, "Strained silicon as a new electro-optic material," *Nature*, vol. 441, pp. 199–202, May 11, 2006.
[8] M. Cazzanelli *et al.*, "Second-harmonic generation in silicon waveguides strained by silicon nitride," *Nature Mater.*, vol. 11, pp. 148–154, Dec. 4, 2011.
[9] N. K. Hon, K. K. Tsia, D. R. Solli, and B. Jalali, "Periodically poled silicon," *Appl. Phys. Lett.*, vol. 94, Mar. 2, 2009, Art. no. 091116.
[10] X. Liu *et al.*, "The DC electric field induced second-order nonlinear susceptibility of silicon crystals," *Proc. SPIE*, vol. 6839, pp. 68391U-1–68391U-5, 2007.
[11] V. A. Margulis, E. A. Gaiduk, and E. N. Zhidkin, "Electric-field-induced optical second-harmonic generation and nonlinear optical rectification in semiconducting carbon nanotubes," *Opt. Commun.*, vol. 183, pp. 317–326, Sep. 1, 2000.
[12] R. E. de Oliveira and C. J. de Matos, "Quasi-phase-matched second harmonic generation in silicon nitride ring resonators controlled by static electric field," *Opt. Exp.*, vol. 21, pp. 32690–32698, Dec. 30, 2013.
[13] M. Dinu, F. Quochi, and H. Garcia, "Third-order nonlinearities in silicon at telecom wavelengths," *Appl. Phys. Lett.*, vol. 82, pp. 2954–2956, May 5, 2003.
[14] X. G. Chen, N. C. Panoiu, and R. M. Osgood, "Theory of Raman-mediated pulsed amplification in silicon-wire waveguides," *IEEE J. Quantum Electron.*, vol. 42, no. 2, pp. 160–170, Jan./Feb. 2006.
[15] I. W. Hsieh *et al.*, "Ultrafast-pulse self-phase modulation and third-order dispersion in Si photonic wire-waveguides," *Opt. Exp..*, vol. 14, pp. 12380–12387, Dec. 11, 2006.
[16] J. I. Dadap *et al.*, "Nonlinear-optical phase modification in dispersion-engineered Si photonic wires," *Opt. Exp.*, vol. 16, pp. 1280–1299, Jan. 21, 2008.
[17] H. F. Wolf, *Silicon Semiconductor Data[M]*: New York, NY, USA: Pergamon, 1969.
[18] W. H. Press, *Numerical Recipes 3rd Edition: The Art of Scientific Computing*. Cambridge, U.K.: Cambridge Univ. Press, 2007.
[19] S. D. Hu, B. Zhang, and Z. J. Li, "A new analytical model of high voltage silicon on insulator (SOI) thin film devices," *Chin. Phys. B*, vol. 18, pp. 315–319, Jan. 2009.
[20] M. S. Rouifed *et al.*, "Low loss SOI waveguides and MMIs at the MIR wavelength of 2 mu m," *IEEE Photon. Technol. Lett.*, vol. 28, no. 24, pp. 2827–2829, Dec. 15, 2016.
[21] P. A. Franken, G. Weinreich, C. W. Peters, and A. E. Hill, "Generation of optical harmonics," *Phys. Rev. Lett.*, vol. 7, pp. 118–119, 1961.
[22] K. Sakai, Y. Koyata, and Y. Hirano, "Planar-waveguide quasi-phase-matched second-harmonic-generation device in Y-cut MgO-doped LiNbO3," *Opt. Lett.*, vol. 31, pp. 3134–3136, Nov. 1, 2006.

[23] J. J. Ju *et al.*, "Quasi-phase-matched second-harmonic generation in nonlinear optical polymer waveguide," *J. Nonlinear Opt. Phys. Mater.*, vol. 13, pp. 383–389, Dec. 2004.
[24] C. Xiong *et al.*, "Integrated GaN photonic circuits on silicon (100) for second harmonic generation," *Opt. Exp.*, vol. 19, pp. 10462–10470, May 23, 2011.
[25] F. De Leonardis, B. Troia, R. A. Soref, and V. M. N. Passaro, "Investigation of mid-infrared second harmonic generation in strained germanium waveguides," *Opt. Exp.*, vol. 24, May 16, 2016.
[26] J. A. Armstrong, N. Bloembergen, J. Ducuing, and P. S. Pershan, "Interactions between light waves in a nonlinear dielectric," *Phys. Rev.*, vol. 127, pp. 1918–1939, 1962.
[27] M. Koselja, J. Kvapil, V. Skoda, J. Kubelka, and K. Hamal, "Linbo3 as an effective SHG for YAP-ND lasers," *Czechoslovak J. Phys.*, vol. 36, pp. 1455–1458, 1986.
[28] M. M. Choy and R. L. Byer, "Accurate 2nd-order susceptibility measurements of visible and infrared nonlinear crystals," *Phys. Rev. B*, vol. 14, pp. 1693–1706, 1976.
[29] S. Lavdas, S. Zhao, J. B. Driscoll, R. R. Grote, R. M. Osgood, and N. C. Panoiu, "Wavelength conversion and parametric amplification of optical pulses via quasi-phase-matched four-wave mixing in long-period Bragg silicon waveguides," *Opt. Lett.*, vol. 39, pp. 4017–4020, Jul. 1, 2014.
[30] J. S. Levy, M. A. Foster, A. L. Gaeta, and M. Lipson, "Harmonic generation in silicon nitride ring resonators," *Opt. Exp.*, vol. 19, pp. 11415–21, Jun. 6, 2011.
[31] U. Willer, M. Saraji, A. Khorsandi, P. Geiser, and W. Schade, "Near- and mid-infrared laser monitoring of industrial processes, environment and security applications," *Opt. Lasers Eng.*, vol. 44, pp. 699–710, Jul. 2006.
[32] M. Ebrahim-Zadeh and K. Vodopyanov, "Mid-infrared coherent sources and applications: introduction," *J. Opt. Soc. Amer. B-Opt. Phys.*, vol. 33, Nov. 1, 2016, Art. no. MIC1.
[33] G. Li, S. Zhang, and T. Zentgraf, "Nonlinear photonic tetasurfaces," *Nature Rev. Mater.*, vol. 2, pp. 17010, Mar. 2017.